Access to Highly Efficient Energy Transfer in Metal-Organic Frameworks via Mixed Linkers Approach.

Access to Highly Efficient Energy Transfer in Metal-Organic Frameworks via Mixed Linkers Approach

Jiangtao Jia,[a¥] Luis Gutiérrez-Arzaluz,[b¥] Osama Shekhah,[a] Norah Alsadun,[a,c] Justyna Czaban-Jóźwiak,[a] Sheng Zhou,[a] Osman M. Bakr,[b] Omar F. Mohammed,[b,*] and Mohamed Eddaoudi[a*]

[a] King Abdullah University of Science and Technology (KAUST), Functional Materials Design, Discovery and Development Research Group (FMD_3), Advanced Membranes and Porous Materials Center (AMPMC), Division of Physical Sciences and Engineering (PSE), Thuwal 23955-6900, Saudi Arabia.

[b] King Abdullah University of Science and Technology (KAUST), Division of Physical Sciences and Engineering (PSE), Thuwal 23955-6900, Saudi Arabia.

[c] Department of Chemistry, College of Science, King Faisal University (KFU), Alahsa 31982-400, Saudi Arabia.

Supporting Information Placeholder

ABSTRACT: Herein, we report a new light-harvesting mixed-ligand Zr(IV)-based metal-organic framework (MOF),with underlying **fcu** topology, encompassing the $[Zr_6(\mu_3\text{-}O)_4(\mu_3\text{-}OH)_4(O_2C\text{–})_{12}]$ cluster and an equimolar mixture of thiadiazole-and imidazole-functionalized ligands. The successful integration of ligands with similar structural features but with notable chemical distinction afforded the attainment of a highly efficient energy transfer. Notably, the very strong spectral overlap between the emission spectrum of benzimidazole (energy donor) and the absorption spectrum of thiadiazole (energy acceptor) provided an ideal platform to achieve very rapid (picosecond time scale) and highly efficient energy transfer (around 90% efficiency), as evidenced by time-resolved spectroscopy. Remarkably, the ultrafast time-resolved experiments quantified for the first time the anticipated close proximity of the two linkers with an average distance of 17 Å. This finding paves the way for the design and synthesis of periodic MOFs affording very efficient and fast energy transfer to mimic natural photosynthetic systems.

Photosynthesis is one of the key processes in nature, and it is principally based on an energy transfer process that takes place between chlorophyll (an antenna molecule) and a carotenoid (a pigment molecule) present in floras. The energy transfer process in plants occurs by means of the absorption of a wide range of wavelengths of sunlight that can be transferred to the reaction center via energy transfer and is then converted into chemical energy.[1-3] Several attempts have been made to design highly efficient natural energy transfer systems, such as assemblies of covalently bonded porphyrin arrays,[4] dendrimers,[5] chromogenic polymers,[6] and self-assembled donor–acceptor supramolecular systems.[7] This energy transfer process is most effective through assembly of an ordered network embedded within the same systems.[8]

Metal–organic frameworks (MOFs), an emerging class of porous crystalline materials, that are built up from multidentate organic building blocks and metal or metal clusters,[9] have paved their way as bulk and thin films in diverse applications, including gas separation and storage,[10] sensing,[11] catalysis,[12] and drug release.[13] This versatility is a result of their permanent porosity, surface area, and structural and functional tunability. In particular, MOFs have been brought into the limelight as a suitable platform for exploration of directional energy transfer phenomena. This is mainly due to the distances and angles between linkers in MOF structures, which can be easily determined by different techniques such as single-crystal X-ray crystallography. The ability to design and fine-tune MOF structures can be approached methodically *via* the unlimited possibilities of altering and combining organic ligands and metals or metal clusters.[14-15]

In recent years, several research groups have made considerable progress in the design and development of MOFs for light-harvesting applications. In principle, energy transfer in MOFs can be introduced via various pathways, including metal-to-ligand, metal-to-metal, host-to-guest, and ligand-to-ligand scenarios.[16-21] Several studies have reported stimulating strut-to-strut energy transfer pathways within MOFs encompassing porphyrin ligands.[22-24] These early investigations encouraged us to explore novel structures containing two complementary ligands in a single MOF structure (mixed-ligand-based MOFs) to study ligand-to-ligand energy transfer. The mixed-ligand approach is the ideal design to co-assemble two ligands in a single MOF structure. Thus, we herein report a new zirconium-based mixed-ligand **fcu** MOF (Zr-ML-**fcu**-MOF), which was obtained by the solvothermal reaction between a zirconium salt and a equimolar mixture ratio of 4,4'-(1H-benzo[d]imidazole-4,7-diyl)dibenzoic acid (**BI**) and 4,4'-(benzo[c][1,2,5]thiadiazole-4,7-diyl)dibenzoic acid (**TD**)[25-26] linkers (see Figure 1). The mixed-ligand strategy successfully yielded Zr-ML-**fcu**-MOF, because of the identical length, symmetry and connectivity of the two ligands (see Figure 1). The rapid and highly efficient ligand-to-ligand energy transfer from the benzimidazole linker to the thiadiazole linker in Zr-ML-**fcu**-MOF was confirmed by various techniques, such as steady-state and time-resolved luminescence measurements.

The new Zr-ML-**fcu**-MOF was synthesized by a conventional method, as described in Figure 1. $ZrCl_4$ and TFA were mixed in DMF for 1 h, followed by the addition of **BI** and **TD** solutions. Heating for 24 h at 120 °C resulted in the formation of Zr-ML-**fcu**-MOF as pale yellow fine crystals. The synthetic procedures are described in detail in the experimental section in the supporting information (SI). For comparison purposes, we have also synthesized single-ligand MOFs (Zr-BI-**fcu**-MOF and Zr-TD-**fcu**-MOF) of **BI** and **TD** by a conventional method, which also yielded white and yellow fine crystal products, respectively. Figure 2a shows the powder X-ray diffraction (PXRD) patterns of the three as-synthesized MOFs. The PXRD

comparison of the three MOFs with UiO-68 calculations confirms that they have the same structure. The PXRD patterns also confirm the presence of pure-phase Zr-ML-**fcu**-MOF, comparable to that of the single-ligand-based MOFs.

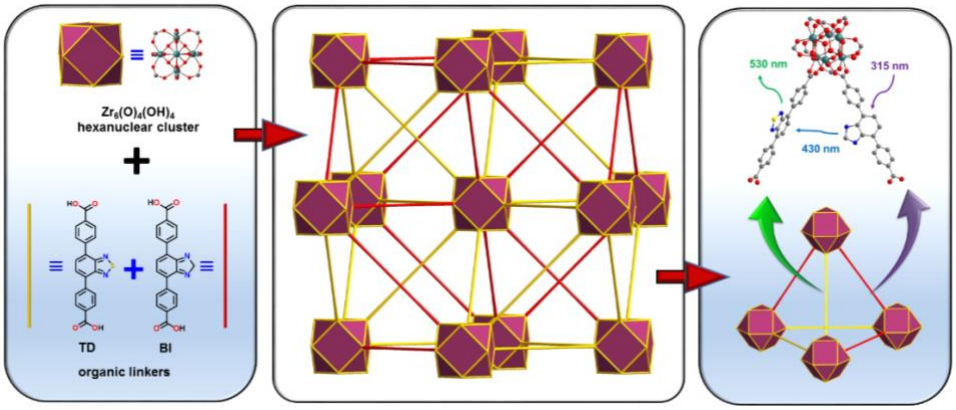

Figure 1. Schematic representation of the Zr-ML-**fcu**-MOF structure and its synthesis from the Zr precursor and the **BI** (represented as yellow line) and **TD** (represented as red line) mixed linkers. (inset) The chemical structure of the Zr-ML-**fcu**-MOF in the tetrahedral cage with the different absorption and emission wavelengths of the two linkers.

^{1}H NMR measurements were conducted to determine the ratio of **BI** and **TD** linkers in these Zr-ML-**fcu**-MOFs. It should be noted that the ^{1}H NMR spectra were obtained after digestion of the Zr-ML-**fcu**-MOF in concentrated hydrochloric acid and separation of the organic ligands by centrifugation. ^{1}H NMR of the digested Zr-ML-**fcu**-MOF shows signals from both ligands. As shown in Figure 1b, the peak at 8.08 ppm could be attributed to the **TD** ligand, and the peak at 7.68 ppm represents the proton from the **BI** ligand. By integrating the peaks from both ligands, we can conclude that the ratio between the **BI** and **TD** ligands is approximately 1:1.25. We also performed high-resolution X-ray photoelectron spectroscopy (XPS) (Figure S5) to determine the nitrogen (N) and sulfur (S) contents on the surface of Zr-ML-**fcu**-MOF. The results show that on the Zr-ML-**fcu**-MOF surface, both N and S are present, and by calculating the ratio of N to S, we can conclude that the ratio of **BI**:**TD** ligands on the surface is approximately 1.1:1, which is very comparable to that determined from the ^{1}H NMR data.

The scanning electron microscopy (SEM) image of the mixed ligand sample (Figure S6) shows that Zr-ML-**fcu**-MOF is mainly composed of one type of very small crystal particle. The elemental mapping scan of N and S for the Zr-ML-**fcu**-MOF particles shows a uniform distribution of N and S, which indicates that there is a good distribution of the two linkers in the MOF structure. From the N and S contents, we estimated the ratio of **BI**:**TD** ligands to be approximately 1:1.1 (Figure S7, and S8). The porosity of Zr-BI-**fcu**-MOF, Zr-TD-**fcu**-MOF, and Zr-ML-**fcu**-MOF was evaluated via nitrogen adsorption–desorption isotherms at 77 K (Figures S9, S10 and S11). All of Zr-BI-**fcu**-MOF, Zr-TD-**fcu**-MOF, and Zr-ML-**fcu**-MOF have shown type I N_2 isotherms. On the other hand, Brunauer–Emmett–Teller (BET) analysis of the N_2 adsorption–desorption isotherms confirms that Zr-BI-**fcu**-MOF, Zr-TD-**fcu**-MOF, and Zr-ML-**fcu**-MOF have high surface areas of ~3490, 2380 and 3110 m^2g^{-1} and pore volumes of 1.47, 1.02 and 1.26 $cm^3\ g^{-1}$, respectively.

The efficient energy transfer in Zr-ML-**fcu**-MOF was visualized using steady-state absorption and photoluminescence (PL), and time-resolved spectroscopies. The steady-state spectra in Figure 3a show that Zr-BI-**fcu**-MOF has an absorption band at 350 nm and exhibits an emission spectrum between 400 and 550 nm. Zr-TD-**fcu**-MOF (Figure 3b) shows a broad absorption spectrum at approximately 450 nm and an emission band at 530 nm. As shown in Figure 3, the significant spectral overlap between the emission spectrum of Zr-BI-**fcu**-MOF (donor) and the absorption spectrum of Zr-TD-**fcu**-MOF (acceptor) strongly supports the energy transfer process from the **BI** linker to the **TD** linker.

Note that in addition to the distance between the two linkers, the degree of this spectral overlap is one of the key factors used to determine the rate and efficiency of Förster-type resonant energy transfer (FRET).[27]

We explore and decipher the interplay between the linkers in Zr-ML-**fcu**-MOF using steady-state absorption experiments, as shown in Figure 3c. Zr-ML-**fcu**-MOF has a broad absorption band from 350 to 500 nm. This spectrum is consistent with contributions from the Zr-BI-**fcu**-MOF band at 350 nm and that from Zr-TD-**fcu**-MOF at approximately 450 nm.

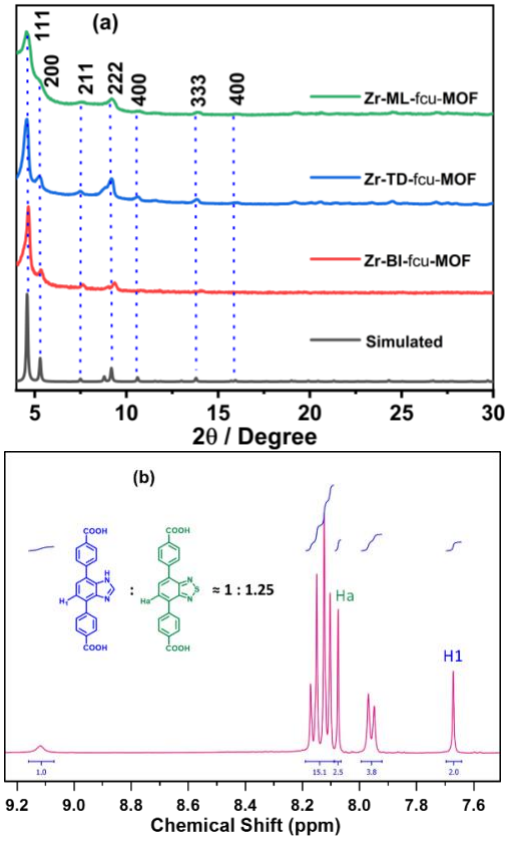

Figure 2. (a) PXRD patterns of the synthesized **Zr-BI**-fcu-**MOF** (red), **Zr-TD**-fcu-**MOF** (blue) and **Zr-ML**-fcu-**MOF** (green) and simulated PXRD pattern of UiO-68 (black); (b) $_1$H NMR plot of the digested **Zr-ML**-fcu-**MOF**.

This observation also confirms the presence of both ligands in the MOF. On the other hand, from the emission spectra of Zr-ML-**fcu**-MOF, we note that the disappearance of the **BI** emission peak upon 315 nm excitation provides an indication for energy transfer from **BI** to **TD**. The almost complete PL quenching of the **BI** emission band indicates that the process occurs in our Zr-ML-**fcu**-MOF with very high efficiency. This behavior is not observed in the physical mixture of free ligands and is not observed in the physically mixed Zr-BI-**fcu**-MOF and Zr-TD-**fcu**-MOF (Figure S12-S14), highlighting the importance of the Zr-ML-**fcu**-MOF architecture that significantly facilitates the process due to the proximity and orientation of the ligands. In other words, the constrain produced by the MOF architecture, facilitates the energy transfer process and prevents other ligand excited-state deactivation channels to take place

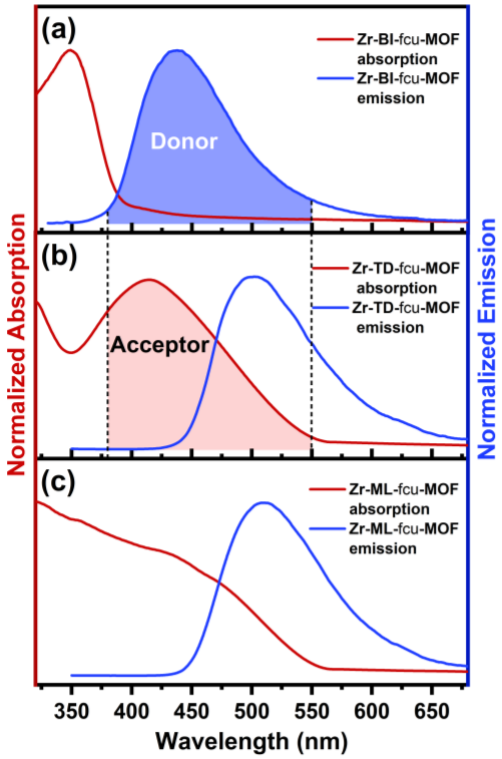

Figure 3. Absorption and emission spectra of **Zr-BI**-fcu-**MOF** (a), **Zr-TD**-fcu-**MOF** (b), and **Zr-ML**-fcu-**MOF** (c) in acetonitrile. λ_{exc} = 315 nm. The framed area shows the overlap between donor emission and acceptor absorption.

To confirm the energy transfer process and determine its characteristic rate, we performed time-resolved emission experiments through time-correlated single-photon counting technique (TCSPC). Namely, the **BI** band was monitored at 440 nm, and the **TD** band was monitored at 530 nm. The TCSPC data in Figure 4 show significant differences in the excited-state lifetimes of Zr-BI-**fcu**-MOF, Zr-TD-**fcu**-MOF, and Zr-ML-**fcu**-MOF. At early times (Figure 4a), the TD band in Zr-ML-**fcu**-MOF (530 nm) shows a PL rise compared with that of the respective single-ligand MOF. This accumulation could be attributed to the energy transfer from the **BI** to the **TD**. The extracted time constant of 108 ± 12 ps and the complete PL quenching of the donor suggest a rapid and highly efficient energy transfer between the two ligands. Complementing this evidence, the 440 nm emission band in Zr-ML-**fcu**-MOF exhibits an early fast decay compared to that of Zr-BI-**fcu**-MOF. It is worth mentioning that this energy transfer rate is faster compared to the ones found in other MOFs that exhibit nanosecond scale ligand-to-ligand energy transfer.[14, 17, 21, 28]

The exponential fittings for the kinetic traces on the long time scale in Figure 4b show a diminution in the BI emission lifetime from 2.82 ± 0.09 ns for Zr-BI-**fcu**-MOF to 0.81 ± 0.06 ns for Zr-ML-**fcu**-MOF. This decrease is accompanied by an increase in the lifetime of the **TD** emission lifetime from 1.41 ± 0.07 ns in Zr-TD-**fcu**-MOF to 3.17 ± 0.06 ns in Zr-ML-**fcu**-MOF. These changes also confirm the photoluminescence quenching of the **BI** by energy transfer to the **TD**.

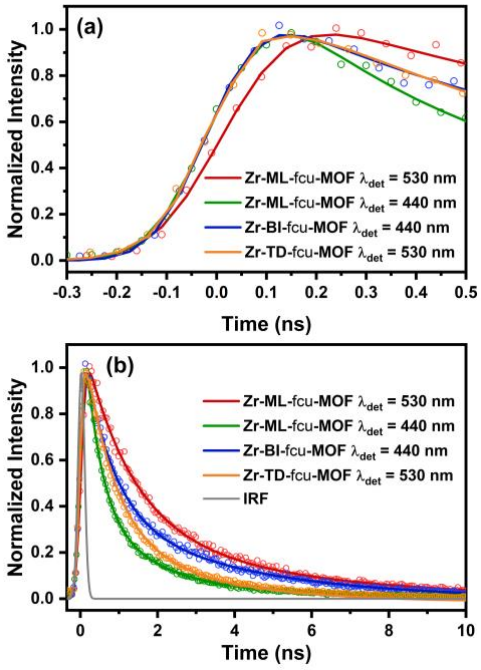

Figure 4. TCSPC data for **Zr-BI**-fcu-**MOF**, **Zr-TD**-fcu-**MOF**, and **Zr-ML**-fcu-**MOF** at their emission bands in acetonitrile solution (a) on an early time scale and (b) on a long time scale. The exponential fittings are indicated as solid lines. λ_{exc} = 350 nm.

Using the lifetime and steady-state spectroscopic data, we first calculated the distance between the **BI** and **TD** ligands inside the Zr-ML-**fcu**-MOF through the Förster energy transfer equation (eq. 1).[27]

$$k_{FRET} = \frac{1}{\tau_D}\left(\frac{R_0}{r}\right)^6 \qquad (1)$$

where k_{FRET} is the rate of the energy transfer process obtained from PL lifetime measurements, τ_D is the lifetime of the donor in the absence of the acceptor, R_0 is the Förster distance, and r is the distance between the donor and the acceptor units. More details about the values of the equation parameters are included in the S I. From the kinetic traces, the energy transfer time constant was determined to be 108 ps (the rise component in the TD kinetic traces in the Zr-ML-**fcu**-MOF). This time constant yielded a length of 17 Å between the two ligands. This value is in good agreement with the calculated values for neighboring ligands inside Zr-**fcu**-MOFs. It should be noted that there are two types of pores in Zr-ML-**fcu**-MOF, octahedral and tetrahedral. The average distances between the two ligands in the tetrahedral and octahedral cages are approximately 12-17 Å and 12-24 Å, respectively (Figure S15). This evidence also confirms that the ligands are evenly well distributed within the Zr-ML-**fcu**-MOF structure. The energy transfer most likely takes place between ligands at close proximity, where the probability of finding different ligands next to each other is high.

The time-resolved PL results also allow us to estimate the efficiency of energy transfer between the two linkers via eq. 2:[29]

$$\epsilon = \frac{1}{1 + \frac{1}{\tau_D k_{FRET}}} \qquad (2)$$

The efficiency (ϵ) found in our system was ~ 90 %. This high value is also consistent with the substantial decrease in the **BI** emission band in the steady-state experiments. Moreover, it confirms the capability of MOFs to serve as excellent light-harvesting materials in addition to all their known properties. It should be noted that the efficiency is higher than other imidazole derivatives MOFs (72 %),[28] and even porphyrin-based MOFs (85 %),[14, 17, 28] establishing our MOF as a better energy-transfer system and a potential light-harvesting material template.

In summary, we have successfully synthesized a new Zr-ML-**fcu**-MOF based on mixed imidazole- and thiadiazole-functionalized linkers. This new MOF structure exhibits very rapid and highly efficient energy transfer. More specifically, steady-state and time-resolved spectroscopic measurements demonstrate that 90 % energy transfer efficiency with an approximately 100 ps time constant was achieved, representing one of the most efficient energy transfer processes in families of MOFs. This work highlights the key variable components to design and synthesize MOFs as new efficient light-harvesting materials. Moreover, since the inter-ligand distance has a remarkable effect on the energy transfer process, the system could be slightly modified to tune its optical properties by controlling the ligand-ligand distance as have been proposed for other systems that undergo variable energy transfer process.[30]

ASSOCIATED CONTENT

Supporting Information

The Supporting Information is available free of charge on the ACS Publications website. Synthesis, experimental data and procedures, X-ray diffraction, absorption and photoluminescence data.

AUTHOR INFORMATION

Corresponding Author

Mohamed Eddaoudi: mohamed.eddaoudi@kaust.edu.sa

Omar F. Mohammed: omar.abdelsaboor@kaust.edu.sa

Author Contributions

¥J.J. and L.G.A contributed equally.

Notes

The authors declare no competing financial interests.

ACKNOWLEDGMENT

The authors gratefully acknowledge financial support from King Abdullah University of Science and Technology (KAUST).

REFERENCES

(1) Barber, J.; Andersson, B., Revealing the Blueprint of Photosynthesis. *Nature* **1994**, *370* (6484), 31-34.
(2) Cheng, Y. C.; Fleming, G. R., Dynamics of Light Harvesting in Photosynthesis. Annu. *Rev. Phys. Chem.* **2009**, *60*, 241-262.
(3) Vangrondelle, R.; Dekker, J. P.; Gillbro, T.; Sundstrom, V., Energy-Transfer and Trapping in Photosynthesis. *Biochim. Biophys. Acta, Bioenerg.*. **1994**, *1187* (1), 1-65.
(4) Aratani, N.; Kim, D.; Osuka, A., Discrete Cyclic Porphyrin Arrays as Artificial Light-Harvesting Antenna. *Accounts. Chem. Res.* **2009**, *42* (12), 1922-1934.
(5) Astruc, D.; Boisselier, E.; Ornelas, C., Dendrimers Designed for Functions: From Physical, Photophysical, and Supramolecular Properties to Applications in Sensing, Catalysis, Molecular Electronics, Photonics, and Nanomedicine. *Chem. Rev.* **2010**, *110* (4), 1857-1959.
(6) Webber, S. E., Photon-Harvesting Polymers. *Chem. Rev.* **1990**, *90* (8), 1469-1482.
(7) Li, X. Y.; Sinks, L. E.; Rybtchinski, B.; Wasielewski, M. R., Ultrafast aggregate-to-aggregate energy transfer within self-assembled light-harvesting columns of zinc phthalocyanine tetrakis(perylenediimide). *J. Am. Chem. Soc*. **2004**, *126* (35), 10810-10811.
8. Wasielewski, M. R., Self-Assembly Strategies for Integrating Light Harvesting and Charge Separation in Artificial Photosynthetic Systems. *Accounts. Chem. Res.* **2009**, *42* (12), 1910-1921.
(9) Furukawa, H.; Cordova, K. E.; O'Keeffe, M.; Yaghi, O. M., The Chemistry and Applications of Metal-Organic Frameworks. *Science* **2013**, *341* (6149), 974-986.
(10) Shekhah, O.; Chernikova, V.; Belmabkhout, Y.; Eddaoudi, M., Metal–Organic Framework Membranes: From Fabrication to Gas Separation. *Crystals* **2018**, *8* (11), 412-467.
(11) Kreno, L. E.; Leong, K.; Farha, O. K.; Allendorf, M.; Van Duyne, R. P.; Hupp, J. T., Metal-Organic Framework Materials as Chemical Sensors. *Chem. Rev.* **2012**, *112* (2), 1105-1125.
(12) De Luna, P.; Liang, W.; Mallick, A.; Shekhah, O.; García de Arquer, F. P.; Proppe, A. H.; Todorović, P.; Kelley, S. O.; Sargent, E. H.; Eddaoudi, M., Metal–Organic Framework Thin Films on High-Curvature Nanostructures Toward Tandem Electrocatalysis. *ACS Appl. Mater. Interfaces* **2018**, *10* (37), 31225-31232.
(13) Horcajada, P.; Chalati, T.; Serre, C.; Gillet, B.; Sebrie, C.; Baati, T.; Eubank, J. F.; Heurtaux, D.; Clayette, P.; Kreuz, C.; Chang, J. S.; Hwang, Y. K.; Marsaud, V.; Bories, P. N.; Cynober, L.; Gil, S.; Ferey, G.; Couvreur, P.; Gref, R., Porous metal-organic-framework nanoscale carriers as a potential platform for drug delivery and imaging. *Nat. Mater.* **2010**, *9* (2), 172-178.
(14) So, M. C.; Wiederrecht, G. P.; Mondloch, J. E.; Hupp, J. T.; Farha, O. K., Metal-organic framework materials for light-harvesting and energy transfer. *Chem. Commun.* **2015**, *51* (17), 3501-3510.
(15) Sava, D. F.; Rohwer, L. E. S.; Rodriguez, M. A.; Nenoff, T. M., Intrinsic Broad-Band White-Light Emission by a Tuned, Corrugated Metal-Organic Framework. *J. Am. Chem. Soc.* **2012**, *134* (9), 3983-3986.
(16) Sun, J. K.; Cai, L. X.; Chen, Y. J.; Li, Z. H.; Zhang, J., Reversible luminescence switch in a photochromic metal-organic framework. *Chem. Commun.* **2011**, *47* (24), 6870-6872.
(17) Kent, C. A.; Mehl, B. P.; Ma, L. Q.; Papanikolas, J. M.; Meyer, T. J.; Lin, W. B., Energy Transfer Dynamics in Metal-Organic Frameworks. *J. Am. Chem. Soc.* **2010**, *132* (37), 12767-12769.
(18) Sun, L. B.; Xing, H. Z.; Liang, Z. Q.; Yu, J. H.; Xu, R. R., A 4+4 strategy for synthesis of zeolitic metal-organic frameworks: an indium-MOF with SOD topology as a light-harvesting antenna. *Chem. Commun.* **2013**, *49* (95), 11155-11157.
(19) Jin, S. Y.; Son, H. J.; Farha, O. K.; Wiederrecht, G. P.; Hupp, J. T., Energy Transfer from Quantum Dots to Metal-Organic Frameworks for Enhanced Light Harvesting. *J. Am. Chem. Soc.* **2013**, *135* (3), 955-958.
(20) Son, H. J.; Jin, S. Y.; Patwardhan, S.; Wezenberg, S. J.; Jeong, N. C.; So, M.; Wilmer, C. E.; Sarjeant, A. A.; Schatz, G. C.; Snurr, R. Q.; Farha, O. K.; Wiederrecht, G. P.; Hupp, J. T., Light-Harvesting and Ultrafast Energy Migration in Porphyrin-Based Metal-Organic Frameworks. *J. Am. Chem. Soc.* **2013**, *135* (2), 862-869.
(21) Lee, C. Y.; Farha, O. K.; Hong, B. J.; Sarjeant, A. A.; Nguyen, S. T.; Hupp, J. T., Light-Harvesting Metal-Organic Frameworks (MOFs): Efficient Strut-to-Strut Energy Transfer in Bodipy and Porphyrin-Based MOFs. *J. Am. Chem. Soc.* **2011**, *133* (40), 15858-15861.
(22) Williams, D. E.; Rietman, J. A.; Maier, J. M.; Tan, R.; Greytak, A. B.; Smith, M. D.; Krause, J. A.; Shustova, N. B., Energy Transfer on Demand: Photoswitch-Directed Behavior of Metal-Porphyrin Frameworks. *J. Am. Chem. Soc*. **2014**, *136* (34), 11886-11889.
(23) Park, J.; Feng, D. W.; Yuan, S.; Zhou, H. C., Photochromic Metal-Organic Frameworks: Reversible Control of Singlet Oxygen Generation. *Angew. Chem. Int. Edit.* **2015**, *54* (2), 430-435.
(24) Park, J.; Jiang, Q.; Feng, D. W.; Zhou, H. C., Controlled Generation of Singlet Oxygen in Living Cells with Tunable Ratios of the Photochromic Switch in Metal-Organic Frameworks. *Angew. Chem. Int. Edit.* **2016**, *55* (25), 7188-7193.
(25) Mallick, A.; El-Zohry, A. M.; Shekhah, O.; Yin, J.; Jia, J. T.; Aggarwal, H.; Emwas, A. H.; Mohammed, O. F.; Eddaoudi, M., Unprecedented Ultralow Detection Limit of Amines using a Thiadiazole-Functionalized Zr(IV)-Based Metal-Organic Framework. *J. Am. Chem. Soc.* **2019**, *141* (18), 7245-7249.
(26) Sk, M.; Biswas, S., A thiadiazole-functionalized Zr(iv)-based metal–organic framework as a highly fluorescent probe for the selective detection of picric acid. *CrystEngComm* **2016**, *18* (17), 3104-3113.
(27) Sahoo, H., Förster resonance energy transfer – A spectroscopic nanoruler: Principle and applications. *J. Photochem. Photobiol., C* **2011**, *12* (1), 20-30.
(28) Dolgopolova, E. A.; Rice, A. M.; Martin, C. R.; Shustova, N. B., Photochemistry and photophysics of MOFs: steps towards MOF-based sensing enhancements. *Chem. Soc. Rev.* **2018**, *47* (13), 4710-4728.
(29) Beljonne, D.; Curutchet, C.; Scholes, G. D.; Silbey, R. J., Beyond Förster Resonance Energy Transfer in Biological and Nanoscale Systems. *J. Phys. Chem. B* **2009**, *113* (19), 6583-6599.
(30) Chen, C.-X.; Wei, Z.-W.; Fan, Y.-N.; Su, P.-Y.; Ai, Y.-Y.; Qiu, Q.-F.; Wu, K.; Yin, S.-Y.; Pan, M.; Su, C.-Y., Visualization of Anisotropic and Stepwise Piezofluorochromism in an MOF Single Crystal. *Chem* **2018**, *4* (11), 2658-2669.

TOC Graphic

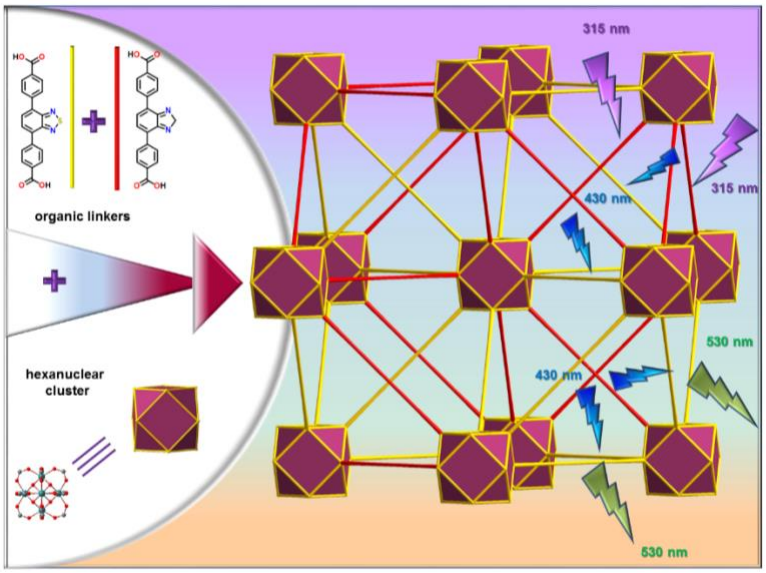
organic linkers
hexanuclear cluster
315 nm
315 nm
430 nm
430 nm
530 nm
530 nm